Electrochemical detection of white spot syndrome virus with a silicone rubber disposable electrode composed of graphene quantum dots and gold nanoparticle-embedded polyaniline nanowires

Kenshin Takemura
Shizuoka University
Jun Satoh
Fisheries Technology Institute of Japan Fisheries Research and Education
Jirayu Boonyakida
Shizuoka University
Sungjo Park
Mayo Clinic College of Medicine and Science
Ankan Dutta Chowdhury
Shizuoka University
Enoch Y. Park (park.enoch@shizuoka.ac.jp)
Shizuoka University https://orcid.org/0000-0002-7840-1424

Research

Keywords: White spot syndrome virus, Electrochemical virus detection, Disposable electrode, Polyaniline, Gold nanoparticle, Graphene quantum dots.

Posted Date: October 13th, 2020

DOI: https://doi.org/10.21203/rs.3.rs-58911/v2

Version of Record: A version of this preprint was published on October 27th, 2020. See the published version at https://doi.org/10.1186/s12951-020-00712-4.

Abstract

Background: With the enormous increment of globalization and global warming, it is expected that the number of newly evolved infectious diseases will continue to increase. To prevent damage due to these infections, the development of a diagnostic method for detecting a virus with high sensitivity in a short time is highly desired. In this study, we have developed a disposable electrode with high-sensitivity and accuracy to evaluate its performances for several target viruses.

Results: Conductive silicon rubber (CSR) was used to fabricate a disposable sensing matrix composed of nitrogen and sulfur-co-doped graphene quantum dots (N,S-GQDs) and a gold-polyaniline nanocomposite (AuNP-PAni). A specific anti-white spot syndrome virus (WSSV) antibody was conjugated to the surface of this nanocomposite, which was successfully applied for the detection of WSSV over a wide linear range of concentration from 1.45×10^2 to 1.45×10 DNA copies/ml, with a detection limit as low as 48.4 DNA copies/ml.

Conclusion: The engineered sensor electrode can retain the detection activity up to 5 weeks, to confirm its long-term stability, required for disposable sensing applications. This is the first demonstration of the detection of WSSV by a nanofabricated sensing electrode with high sensitivity, selectivity, and stability, providing as a potential diagnostic tool to monitor WSSV in the aquaculture industry.

Background

White spot syndrome virus (WSSV) infects shrimp and causes white spot disease (WSD), which is considered one of the most lethal virus pathogens in cultured shrimp [1]. WSSV was initially discovered in Taiwan and spread quickly to the entire world [2, 3]. The infection reaches a cumulative mortality of up to 100% within 10 d, causing rapid economic damage in fishery industries [4]. Recently, India reported an approximately several million US$ loss per year due to WSD [5]. WSSV spreads by vertical infection or cannibalism between shrimp and other invertebrate aquatic organisms, such as crab and crayfish [6], with a high mortality rate; a promising rapid detection method needs to be developed to prevent the onset of this epidemic.

Vaccination is always the most useful method for solving any viral infection. Using WSSV envelope proteins (e.g., VP19 and VP28), a few attempts to induce an immune response and protect shrimp from WSSV infection have already been reported [7–9]. However, the outcome of the vaccination method is still poor considering its practical use. To avoid the risk of WSD in shrimp farming, the only way is to quickly identify the infected shrimp and isolate it from the farm. Current methods for detecting WSSV rely on PCR techniques using viral DNAs or protein assays using a specific antibody [10, 11]. The limit of detection (LOD) is a few hundred DNA copies/ml within 4 to 12 h [12–14]. Likewise, dot blots, lateral flow assay, and enzyme-linked immunosorbent assay (ELISA) using antigen-antibody reactions have been generally used for the detection of WSSV envelope proteins [15–19]. The LOD is in the range of 1000 DNA copies/ml using the lateral flow assay and 120 ng/ml using ELISA. However, the availability of diagnostic

PCR assays for use in aquaculture remains limited because they are costly and require highly skilled operators.

On the other hand, antigen detection methods are useful for rapid clinical diagnosis of viral infection [20] but fail to attain the desired sensitivity. In a recent study, a fluorescence resonance energy transfer (FRET)-based detection technique using graphene oxide detected WSSV with an LOD of 10 DNA copies/ml [21]. In another study, WSSV was detected with an LOD of 1.36×10^3 DNA copies/µl using the electrochemical property of methylene blue conjugated to graphene oxide [22]. Although a few reports on WSSV detection with low sensitivity have been published, in terms of their stability and reliability, these sensors are not suitable for real-time applications.

Nanomaterials with unique physical, optical and electrochemical properties [23, 24] have shown successful detection of viruses with high sensitivity [25–27]. Previously, we demonstrated hepatitis E virus detection with a fabricated biosensor electrode constituted by specific antibodies and nanomaterials based on an engineered impedimetric process [30]. In this report, we have developed a conducting sensor matrix fabricated with polyaniline, nitrogen and sulfur-codoped graphene quantum dots (N,S-GQDs) and gold nanoparticles (AuNPs) for the detection of WSSV. In an interfacial reaction, AuNPs embedded in polyaniline nanowires (AuNP-PAni) were synthesized and bound to N,S-GQDs via the Au-S affinity because the interaction between PAni and AuNPs provides excellent conductivity to the N,S-GQD@AuNP-PAni nanocomposite [28, 29]. The nanocomposite was deposited on a finely electropolymerized polyaniline-coated conductive silicon rubber (CSR) surface. The coating of the Ab-N,S-GQD@AuNP-PAni nanocomposite on the surface of the CSR significantly improved the conductivity of the CSR. On the other hand, the conductivity significantly decreased after capturing WSSV due to the increased charge transfer resistance (R_{ct}) of the Ab-N,S-GQD@AuNP-PAni-coated electrode. This disposable electrode demonstrates the capability for detecting WSSV over a wide linear range with high specificity and sensitivity. The sensor stability was also tested over more than one month to confirm its applicability for on-site virus detection. Thus, our fabricated disposable electrode modified by a simple and uniform nanocomposite coating aiming for more convenient use allows accurate WSSV detection and is applicable to sensing WSSV in the aquaculture industry.

Materials And Methods

Materials

PBS buffer, polyoxyethylene (20) sorbitan monolaurate (Tween 20), sodium acetate, hydrogen peroxide, sulfuric acid, methanol, potassium hydroxide (KOH), chloroform and acetone were purchased from Wako Pure Chemical Ind. Ltd. (Osaka, Japan). $HAuCl_4$, N-(3-dimethylaminopropyl)-N'-ethylcarbodiimide hydrochloride (EDC), N-hydroxysuccinimide (NHS), and bovine serum albumin (BSA) were purchased from Sigma Aldrich Co., LLC (Saint Louis, MO, USA). Oleic acid was purchased from Nacalai Tesque Inc. (Kyoto, Japan). Tetramethylbenzidine (TMBZ) was purchased from Dojindo Laboratories (Kumamoto, Japan). Anti-WSSV VP28 antibody [ab26935] and a mouse monoclonal antibody [B219M] were

purchased from Abcam Inc. (Cambridge, UK). Anti-HA antibody (New Caledonia/20/99) (H1N1) was purchased from Prospec-Tany Techno Gene Ltd. (Rehovot, Israel). Goat anti-rabbit IgG-HRP was purchased from Santa Cruz Biotechnology (CA, USA). Geno type 3 hepatitis E virus (HEV), rabbit anti-G3 HEV IgG antibody, and norovirus-like particle (NoV-LP) were provided by Dr Tian-Cheng Li (National Institute of Infectious Diseases, Japan). Zika virus (ZIKV) strain PRVABC-59 was provided by Professor Kouichi Morita (Institute of Tropical Medicine, Nagasaki University, Japan).

Equipment

UV/vis absorption and fluorescence emission measurements were carried out using a filter-based multimode microplate reader (Infinite® M200; TECAN, Ltd, Männedorf, Switzerland). Transmission electron microscopy (TEM) images were obtained with a TEM system (JEM-2100F; JEOL, Ltd., Tokyo, Japan) operated at 100 kV. Scanning electron microscopy (SEM) images were obtained with SEM equipment (JSM-6510LV; JEOL, Tokyo, Japan). A General Laboratory Homogenizer (OMNI International, USA) was used for WSSV sample preparation from shrimp. Western blotting was carried out using a Trans-Blot-SD (Bio-Rad, Japan) and transferred by using Immobilon ECL Ultra Western HRP Substrate (Merck, Japan). The membrane after western blotting was filmed by a VersaDoc 4000 MP (Bio-Rad, Japan). The centrifugation for virus sample collection proceeded using a Micro-cooled Centrifuge 3700 (KUBOTA, Japan). Powder X-ray diffraction (PXRD) analysis was carried out using a RINT ULTIMA XRD (Rigaku Co., Tokyo, Japan) with a Ni filter and a Cu-Ka source. Data were collected over 2theta = 5–60° at a scan rate of 0.01°/step and 10 s/point. Zeta potential and dynamic light scattering (DLS) measurements were performed using a Zetasizer Nano series (Malvern Inst. Ltd., Malvern, UK). Conjugation of the Ab to the QDs and GNPs was confirmed with a plate reader (Bio-Rad, model 680, Hercules, USA). A high-resolution transmission electron microscopy (HRTEM) image was taken by a JEM-2100F at 200 kV (JEOL, Tokyo, Japan). Atomic force microscopy (AFM) analysis was achieved with a Nanoscope IV PicoForce Multimode atomic force microscope (Bruker, Santa Barbara, CA, USA) in contact mode [31]. Electrochemical cyclic voltammetry (CV) and electrochemical impedance spectroscopy (EIS) were carried out using an SP-150 (BioLogic Inc, Tokyo, Japan) in a conventional three-electrode cell consisting of platinum wire. Saturated Ag/AgCl was used as an electrolyzer (EC frontier, Tokyo, Japan).

Synthesis of the AuNP-PAni nanocomposite

AuNP-PAni was synthesized using the interfacial polymerization method [29]. A 0.5 M aniline monomer in toluene mixture was prepared as an organic phase, and 3 mM $HAuCl_4$ in 0.1 M HCl solution was slowly poured in as an aqueous phase to initiate the interfacial polymerization process. Polyaniline nanowires were gradually formed by oxidation of aniline into an aqueous phase, and the solution color became dark green within several minutes. At the same time, $HAuCl_4$ was reduced to AuNPs and embedded within the polyaniline nanowires. The synthesized solution was centrifuged (room temperature, 5500 × g) and redispersed using ultrapure water for purification. This purification process was repeated 3 times.

N,S-GQD preparation and conjugation of anti-WSSV VP28 antibody

N,S-GQDs were synthesized using a hydrothermal system [32]. N,S-GQDs were quickly bonded with anti-WSSV VP28 antibody (Ab) using EDC/NHS covalent chemistry [33]. In brief, 0.1 M EDC was mixed with a solution containing Ab 5.1 µg, and EDC reacted with the carboxyl group of the Ab to create an active-ester intermediate within 30 min of stirring at 7°C. To generate amine reactivity of the amino group with the surface of the GQDs, 0.1 M NHS and 1 ml of N,S-GQDs were added and continuously stirred at 7°C over 16 h. The reaction solution was dialyzed using a 1 kDa dialysis bag to remove unreacted EDC and NHS. Finally, the solution of Ab-conjugated N,S-GQDs (Ab-N,S-GQDs) was preserved in 0.1 M PBS (pH 7.4) at 4°C until use.

The conjugation of Abs to N,S-GQDs was confirmed using ELISA. Ab-conjugated N,S-GQDs were added to a polystyrene 96-well plate (100 µl) and incubated overnight at 4°C. As a negative control, 100 µl of BSA was added to a separate well, and 100 µl of 5% skim milk solution was added and applied as a blocking agent after washing 3 times with PBST (containing 1 ml of Tween in 999 ml of PBS buffer). After blocking, the 5% skim milk was removed by washing 3 times with PBST. Anti-rabbit IgG-horseradish peroxidase was diluted to 1:4000 with 2% BSA, and 100 µl of this solution was added to the well and incubated at ambient temperature for 1 h. TMB (100 µl), a chromogenic substrate, was added to the well as a coloring reagent, and the solution appeared blue due to the reaction. The reaction was then stopped by adding 50 µl of 10% H_2SO_4, which changed the color of the solution from blue to yellow. The absorbance of the solution was measured using a microplate reader at 450 nm with a reference filter of 655 nm.

Fabrication of the disposable electrode

In ultrapure water, 0.5 M sulfuric acid and 0.1 M aniline monomer were mixed for electrochemical deposition of polyaniline on conductive silicone rubber (CSR) by cyclic voltammetry (CV) in a three-electrode system. The CV curve was recorded at a scan rate of 20 mV/s in a potential range of 0 – 1 V for 15 cycles. The backside of the CSR electrode was covered by nonconducting tape to protect the polyaniline coating on the other side. Then, 15 µl of Ab-N,S-GQD@AuNP-PAni solution was drop-cast on the polymerized CSR/PAni. The formation of the Ab-N,S-GQD@AuNP-PAni nanocomposite was characterized by TEM and XRD.

WSSV collection and pretreatment

A WSSV suspension was prepared according to a previously reported protocol [34]. In brief, the muscle tissue of moribund WSSV-infected shrimp was homogenized using GLH in 4×PBS volume, followed by centrifugation at 1000 × g for 10 min at 4°C. The supernatant was then filtered through a 0.22 µm cellulose acetate membrane. The filtrate containing WSSV was kept at –80°C before use in subsequent experiments.

Detection of WSSV using the disposable electrode

The WSSV solution was diluted in series from 1.0×10^9 DNA copies/ml to 10 DNA copies/ml using filtered 0.1 M PBS. Ten microliters of WSSV solution was dropped on the disposable electrode and incubated for 10 min at room temperature. Ab-N,S-GQD@AuNP-PAni binds the target viruses because of the conjugation of anti-WSSV VP28 antibody (Ab) to N,S-GQDs. The electrode was mildly washed by dipping it in PBST to remove unbound viruses and then placed in an electrolytic solution. The charge resistance value (R_{ct}) on the electrode was measured in the potential electrochemical impedance spectroscopy (PEIS) mode with a sinusoidal amplitude of 5 mV within a frequency range from 100 kHz to 0.1 Hz. The WSSV detection time using this disposable electrode was less than 15 min.

Western blot analysis of WSSV-VP28

The resultant supernatants of WSSV were loaded on an 18% polyacrylamide gel under denatured conditions and transferred to a PVDF membrane using the Trans-Blot-SD system for 1 h at 15 mA. The membrane was then incubated in a blocking buffer (5% w/v skim milk in TBS containing 0.1% Tween 20 [TBS-T]) for 1 h at room temperature, followed by washing the membrane with TBS-T 3 times for 5 min. For protein detection, the membrane was incubated with a primary antibody, anti-WSSV-VP28 rabbit monoclonal antibody (1:2000), overnight at 4°C and washed with TBS-T, followed by incubation with a secondary antibody (anti-IgG [Rabbit] pAb-HRP [1:10000]) for 1 h at room temperature. The immunoreactive bands were visualized and filmed for analysis.

Selectivity and stability of the disposable electrode

IFV A (H1N1) and hepatitis E virus (HEV) were used for the selectivity test of the Ab-N,S-GQD@AuNP-PAni/CSR electrode. To confirm the stability, the disposable electrodes were preserved at 4°C for 60 d, testing the performance of the electrodes every week.

Results And Discussion

Characterization of Ab-N,S-GQD@AuNP-PAni on the CSR

The AuNP-PAni nanocomposite was deposited on a finely electropolymerized polyaniline-coated CSR electrode to form a AuNP-PAni/PAni||CSR electrode. The Ab-N,S-GQDs were then bound to the AuNP-PAni to prepare Ab-N,S-GQD@AuNP-PAni/PAni/CSR as shown in Scheme 1. In the N,S-GQD@AuNP-PAni nanocomposite, the AuNPs play an anchoring role between the N,S-GQDs and the polyaniline wires via soft acid – soft base interactions between Au and S. According to the TEM analysis, the diameter of the AuNP-PAni nanowires was 50 – 70 nm. Additionally, the AuNPs dispersed evenly in the polymeric chain, and their size ranged from 6 – 14 nm (Fig. 1A). The HRTEM image of the N,S-GQD@AuNP-PAni nanocomposite shows two distinct fringe patterns (Fig. 1B) of two crystalized structures of N,S-GQDs, and the AuNPs are deciphered as shown in Fig. 1C. The characteristic fringe of 0.24 nm for AuNPs is deciphered as them being adjacent to the N,S-GQDs with a fringe distance of 0.21 nm, which is the distinctive fringe of the carbon lattice (Fig. 1C) [35, 36].

The structural properties of the N,S-GQD@AuNP-PAni nanocomposite were analyzed by XRD, as shown in Fig. 1D. AuNP peaks are observed in the nanocomposite along with the characteristic peaks at 2θ = 23.6°, 25.5°, 28.2°, 38.2°, 44.3°, 64.4°, and 78.2° corresponding to the (100), (110), (111), (200), (220), and (221) planes, respectively (Fig. 1D) [37, 38]. After the N,S-GQDs were bound, the nanocomposite showed similar peaks and intensities, which indicates that the attachment of GQDs does not induce any structural changes of the AuNPs [39]. The graphitic layer shows a hump at 24° in the XRD spectrum, which is completely masked by the high-intensity peaks of AuNPs. The conjugation of antibody on the N,S-GQDs was confirmed by ELISA. The absorbance value significantly increased after conjugation of the antibody, which confirms the conjugation of Ab-N,S-GQDs (Fig. 1E).

The electrochemical properties of the CSR electrode surface were measured by cyclic voltammetry. Despite the functional conducting matrix, the charge storage capacity of the bare CSR is very low, and the bare CSR shows a narrow curve, which significantly increases after the polyaniline coating (Fig. 1F). Additionally, a redox peak of polyaniline appears at + 0.8/+ 0.1 V, indicating the formation of the emeraldine salt of polyaniline [40]. After the formation of the nanocomposite, the conductivity of the disposable electrode shows an enhancement of the current density, indicating successful preparation of the sensor electrode for electrochemical analysis.

Optimization of the sensing performance of Ab-N,S-GQD@AuNP-PAni

The thickness of the nanocomposite layer on the CSR matrix is an essential parameter for maintaining the reproducibility of a disposable electrode. The thickness of the base matrix of polyaniline is directly proportional to the CV cycle number in the electropolymerization step. The resistance of the polyaniline-coated CSR becomes the lowest at 15 cycles and increases after 20 cycles (Fig. S1) due to overoxidation. This result indicates that a thick polyaniline layer can lead to a reverse effect on the conductivity of CSR. The stability of the 15 cycled PAni/CSR was tested over 50 cycles, showing excellent stability under the optimized polyaniline layer condition (Fig. S2). The thickness of the layer was characterized by SEM and AFM. The bare CSR with a smooth surface becomes rough with coating of polymerized polyaniline (Fig. 2A—B). The roughness of the polyaniline layer-coated CSR becomes smoother again after drop-casting Ab-N,S-GQD@AuNP-PAni to microscale order (Fig. 2C). A similar observation was noted in the corresponding AFM images, as presented in Fig. 2D—E. The rough surface of CSR becomes relatively smooth after the formation of nanoconjugates, following the same trend as the SEM images. The usefulness of AuNP-PAni as a highly conductive material was compared with that of CSR modified with AuNPs (Fig. S3). A standard layer method was used for AuNP modification. In this study, the electric resistance was used as an indicator, and it was shown that AuNPs are a suitable material for this purpose because they lead to higher conductivity by forming a complex with polyaniline nanowires.

After optimizing the PAni electropolymerization and thickness of the sensor electrode, the changes in the electrochemical properties were investigated by EIS. The conductivity and dielectric properties of the CSR surface gradually decreased after polyaniline and Ab-N,S-GQD-AuNP-PAni attachment (Fig. 2F), indicating successful formation of a sensor electrode suitable for virus detection.

Furthermore, the sensing area was optimized for virus detection. Electrodes with different sensor areas from 2 mm² to 25 mm² were prepared, and WSSV was detected by following the same procedure (Fig. S4). The larger the sensor area was, the more remarkable the change in the Rct value. The size of the sensing area indicates the size of the contact surface with the virus during the antigen-antibody reaction. It was suggested that the larger the area is, the more virus that binds to the sensor.

On the other hand, the sensor with a large area has a low correlation coefficient (R^2 value) and a high error range, particularly in the high concentration range. As the area increases, it is difficult to obtain uniformity between electrodes with simple modification by only dropping nanomaterials, resulting in a low R^2 value in virus detection. The electrode with a sensing area of 10 mm², which gave the most reliable result, was used as the optimum detection electrode.

Detection of WSSV

The Nyquist impedance plots of the disposable electrode after incubation of different concentrations of the virus from 10^2 –10^9 copies/ml are shown in Fig. 3A. The EIS responses of the sensor electrodes increase with the concentration of WSSV due to the high resistance accumulation between the virus-loaded nanocomposite and CSR. When WSSV binds to the sensing electrode, a large number of nonconducting virus particles cover the conducting surface of Ab-N,S-GQD@AuNP-PAni/CSR, increasing the charge transfer resistance (R_{ct}). The percentage change of the signal difference between the R_{ct} values of the corresponding virus-loaded electrode and the bare electrode was adopted as the measurement signal. The calibration plot displays an excellent linear relationship between R_{ct} and the WSSV concentration (Fig. 3B). The LOD was 48.4 copies/ml, calculated by 3σ/S (S is the slope of the linear calibration plot, and σ is the unbiased standard deviation from the lowest signal of the detection result) [41]. This value is extremely low and sensitive enough to detect the real analyte [42]. After WSSV detection, the surface of the virus-loaded electrode exhibited a significantly increased roughness, indicating the presence of WSSV on the electrode (Fig. S5).

Selectivity and stability of the disposable electrode

As the antibody-conjugated nanocomposite governs the interaction between the analyte and the sensor electrode, the sensor should possess high selectivity. However, the specificity of the sensor for its real application is still significant for clarifying any possible cross-reactivity. To confirm the specificity for WSSV, various viruses were tested. The sensor responses, except for WSSV (Fig. 4A), were similar to that of the bare electrode, indicating the sensor specificity for the target virus.

The stability of the disposable electrode was tested for 8 weeks to observe its applicability for long-term usage. As depicted in Fig. 4B, the signal intensity of Rct after loading of 104 copies/ml virus remained at 86% until 35 d. However, it dropped to 73.4% after 56 d of storage. This result indicates that the performance of this electrode is 13.8% decreased after 5 weeks of storage. The sensing performance was

significantly decreased after 5 weeks due to degradation of the antibody rather than deterioration of the nanocomposite, which was stable for 6 weeks.

In this work, a disposable electrode was fabricated on a CSR matrix using a Au-PAni-N,S-GQD nanocomposite conjugated with an anti-WSSV antibody for the detection of WSSV. The antigen-antibody interaction has been applied for specific target binding, which generates an EIS-based signal. To extend its application to other types of analytes, we prepared two different electrodes conjugated with different anti-HEV and anti-HA antibodies and detected their corresponding target viruses. The results demonstrate that the Nyquist impedance in both cases increases with increasing virus concentration (Fig. S6A and B), and their corresponding calibration lines show excellent linearity (Fig. S7A and B). The limit of detection was calculated as 34.6 DNA copies/ml for G3 HEV and 0.98 fg/ml for influenza virus A.

Real virus analysis

After successful detection of WSSV in a buffer medium, real samples were collected from 10 WSSV-infected shrimp and tested with the sensor. Their DNA copy numbers were measured by standard RT-PCR and then compared with the results obtained from this electrochemical detection technique. The detection results are summarized in Table 1 and Fig. 5A. According to the RT-PCR data, sample Nos. 2 and 4 do not contain any virus, showing 2.4 and 6.5 copies/ml according to our electrochemical method, and can be ignored. The electrochemical detection results for sample Nos. 8 and 9 significantly deviate from the RT-PCR results. However, the overall trend of the RT-PCR results for the samples shows excellent similarity to the trend of the electrochemical sensor results, confirming the reproducibility of the sensor. In the western blot analysis, the virus titer above 10^7 copies/ml shows VP-28 protein bands at approximately 22 kDa (Fig. 5B), but less than 10^7 copies/ml could not be detected (Table 1). This indicates that our sensing system shows a 6–7 order of magnitude higher sensitivity than western blot. Although the correlation coefficient between the two methods is 90%, the developed method can be used to judge WSSV infection in a short time with easy handling.

Table 1. Details of the detection results for real sample detection using the electrochemical method and RT-PCR.

Sample No	R_{ct} value±SD (n=3)	WSSV concentration (DNA copies/ml)		VP28 detection	Shrimp
		by EIS*	by RT-PCR		
Control	2680±146	0	–		
1	7179±238	4.8×10³	1.2×10□	no	live
2	2797±72	2.4×10□	0	no	live
3	8988±108	2.0×10⁴	6.2×10□	no	dead
4	4572±143	6.5×10□	0	no	live
5	12101±490	2.6×10□	8.4×10□	no	dead
6	16946±406	1.4×10□	9.6×10□	yes	dead
7	26949±140	4.7×10¹□	2.2×10¹□	yes	dead
8	18946±893	6.9×10□	7.5×10□	yes	dead
9	22308±195	1.0×10□	3.5×10□	yes	dead
10	13988±406	1.2×10□	2.4×10□	yes	dead

* The copy number of WSSV was determined from the calibration line (Fig. 3C) using the measured R_{ct} value.

Conclusion

A disposable electrode consisting of an Ab-N,S-GQD@AuNP-PAni nanocomposite on a CSR electrode was fabricated in this work for the detection of WSSV. This disposable sensor showed a low R_{ct} value in the impedance spectrum as a bare sensor, which significantly increased in relation to the target virus concentration over a wide linear range from 10^2 to 10^9 DNA copies/ml, with an LOD of 48.4 copies/ml. The applicability of the proposed disposable electrode was successfully demonstrated, with a high selectivity and a long-term stability of 5 weeks. The sensing capability was also tested for other viruses, indicating its versatile applicability for future usage. The sensor was applied to detect the real WSSV from WSSV-infected shrimp in aquaculture and found to be comparable with RT-PCR, which confirmed its applicability as an excellent monitoring system for real-time virus detection.

Declarations

Availability of data and materials

All data generated or analyzed during this study are included in this manuscript and its supplementary information.

Acknowledgments

We thank Dr. Tian-Cheng Li of the National Institute of Infectious Diseases (Japan) for providing HEV, rabbit anti-G3 HEV IgG antibody, and NoV-LP. We also appreciate Professor Kouichi Morita of the Institute of Tropical Medicine, Nagasaki University (Japan) for kindly providing ZIKV (strain PRVABC-59).

Funding

This work was supported by the Yanmar environmental sustainability support association (YESSA).

Author information

Authors details

[1] Laboratory of Biotechnology, Department of Bioscience, Graduate School of Science and Technology, Shizuoka University, 836 Ohya, Suruga-ku, Shizuoka 422-8529, Japan. [2] National Research Institute of Aquaculture, Japan Fisheries Research and Education Agency, Saiki, Oita, Japan. [3] Division of Cardiovascular Diseases, Mayo Clinic College of Medicine and Science, Mayo Clinic, 200 First Street SW, Rochester, MN, 55905, USA. [4] Laboratory of Biotechnology, Research Institute of Green Science and Technology, Shizuoka University, 836 Ohya, Suruga-ku, Shizuoka 422-8529, Japan.

Contributions

KT performed the sensor design and experiment, data analysis, and writing of the manuscript draft. JS provided the WSSV-infected shrimp and performed data validation. JB performed sample pretreatment and western blotting. SP performed AFM imaging and data validation. ADC contributed to the manuscript preparation, data validation and revision of the manuscript. EYP supervised, funded, and revised the manuscript. All authors approved the final manuscript.

Corresponding author

Correspondence to Enoch Y. Park

Ethics declarations

Ethics approval and consent to participate

Not applicable.

Consent for publication

Not applicable.

Competing interests

The authors declare that they have no competing interests.

References

1. Lo C-F, Ho CH, Peng SE, Chen CH, Hsu HC, Chiu YL, Chang CF, Liu KF, Su MS, Wang CH. White spot syndrome baculovirus (WSBV) detected in cultured and captured shrimp, crabs and other arthropods. Dis Aquat Organ. 1996;27:215–25.
2. Cai S, Huang J, Wang C, Song X, Sun X, Yu J, Zhang Y, Yang C. Epidemiological studies on the explosive epidemic disease of prawn in 1993–1994. J Fish China. 1995;19:112–9.
3. Lo C-F, Kou G-H. Virus-associated white spot syndrome of shrimp in Taiwan: a review. Fish Pathol. 1998;33:365–71.
4. Rajendran K, Vijayan K, Santiago T, Krol R. Experimental host range and histopathology of white spot syndrome virus (WSSV) infection in shrimp, prawns, crabs and lobsters from India. J Fish Dis. 1999;22:183–91.
5. Kalaimani N, Ravisankar T, Chakravarthy N, Raja S, Santiago T, Ponniah A. Economic losses due to disease incidences in shrimp farms of India. Fish Technol. 2013;50:80–6.
6. Wang Y-C, Lo C-F, Chang P-S, Kou G-H. Experimental infection of white spot baculovirus in some cultured and wild decapods in Taiwan. Aquaculture. 1998;164:221–31.
7. Witteveldt J, Cifuentes CC, Vlak JM, van Hulten MC. Protection of Penaeus monodon against white spot syndrome virus by oral vaccination. J Virol. 2004;78:2057–61.
8. Taengchaiyaphum S, Nakayama H, Srisala J, Khiev R, Aldama-Cano DJ, Thitamadee S, Sritunyalucksana K. Vaccination with multimeric recombinant VP28 induces high protection against white spot syndrome virus in shrimp. Dev Comp Immunol. 2017;76:56–64.
9. Witteveldt J, Vlak JM, van Hulten MC. Protection of Penaeus monodon against white spot syndrome virus using a WSSV subunit vaccine. Fish Shellfish Immunol. 2004;16:571–9.
10. Hsu H-C, Lo C-F, Lin S-C, Liu K-F, Peng S-E, Chang Y-S, Chen L-L, Liu W-J, Kou G-H. Studies on effective PCR screening strategies for white spot syndrome virus (WSSV) detection in Penaeus monodon brooders. Dis Aquat Organ. 1999;39:13–9.
11. Nunan LM, Lightner DV. Optimized PCR assay for detection of white spot syndrome virus (WSSV). J Virol Methods. 2011;171:318–21.
12. Nunan LM, Lightner DV. Development of a non-radioactive gene probe by PCR for detection of white spot syndrome virus (WSSV). J Virol Methods. 1997;63:193–201.
13. Yan D-C, Dong S-L, Huang J, Yu X-M, Feng M-Y, Liu X-Y. White spot syndrome virus (WSSV) detected by PCR in rotifers and rotifer resting eggs from shrimp pond sediments. Dis Aquat Organ. 2004;59:69–73.
14. Durand S, Lightner DV. Quantitative real time PCR for the measurement of white spot syndrome virus in shrimp. J Fish Dis. 2002;25:381–9.

15. Dai H, Gao H, Zhao X, Dai L, Zhang X, Xiao N, Zhao R, Hemmingsen SM. Construction and characterization of a novel recombinant single-chain variable fragment antibody against white spot syndrome virus from shrimp. J Immunol Methods. 2003;279:267–75.
16. Zhan WB, Wang YH, Fryer JL, Okubo K, Fukuda H, Yu KK, Meng QX. Production of monoclonal antibodies (MAbs) against white spot syndrome virus (WSSV). J Aquat Anim Health. 1999;11:17–22.
17. Kulabhusan PK, Rajwade JM, Hameed AS, Paknikar KM. Lateral flow assay for rapid detection of white spot syndrome virus (WSSV) using a phage-displayed peptide as bio-recognition probe. Appl Microbiol Biotechnol. 2017;101:4459–69.
18. Kulabhusan PK, Rajwade JM, Sugumar V, Taju G, Hameed AS, Paknikar KM. Field-usable lateral flow immunoassay for the rapid detection of white spot syndrome virus (WSSV). PLoS One. 2017;12:e0169012.
19. Tang X, Liang Q, Liu L, Sheng X, Xing J, Zhan W. An optimized double-antibody sandwich ELISA for quantitative detection of WSSV in artificially infected crayfish. J Virol Methods. 2018;251:133–8.
20. Sithigorngul W, Rukpratanporn S, Pecharaburanin N, Longyant S, Chaivisuthangkura P, Sithigorngul P. A simple and rapid immunochromatographic test strip for detection of white spot syndrome virus (WSSV) of shrimp. Dis Aquat Organ. 2006;72:101–6.
21. Waiwijit U, Phokaratkul D, Kampeera J, Lomas T, Wisitsoraat A, Kiatpathomchai W, Tuantranont A. Graphene oxide based fluorescence resonance energy transfer and loop-mediated isothermal amplification for white spot syndrome virus detection. J Biotechnol. 2015;212:44–9.
22. Natarajan A, Devi KS, Raja S, Kumar AS. An elegant analysis of white spot syndrome virus using a graphene oxide/methylene blue based electrochemical immunosensor platform. Sci Rep. 2017;7:46169.
23. Jain PK, Huang X, El-Sayed IH, El-Sayed MA. Review of some interesting surface plasmon resonance-enhanced properties of noble metal nanoparticles and their applications to biosystems. Plasmonics. 2007;2:107–18.
24. Lee J, Takemura K, Park E. Plasmonic nanomaterial-based optical biosensing platforms for virus detection. Sensors. 2017;17:2332.
25. Lee J, Morita M, Takemura K, Park EY. A multi-functional gold/iron-oxide nanoparticle-CNT hybrid nanomaterial as virus DNA sensing platform. Biosens Bioelectron. 2018;102:425–31.
26. Sepunaru L, Plowman BJ, Sokolov SV, Young NP, Compton RG. Rapid electrochemical detection of single influenza viruses tagged with silver nanoparticles. Chemical science. 2016;7:3892–99.
27. Dick JE, Hilterbrand AT, Boika A, Upton JW, Bard AJ. Electrochemical detection of a single cytomegalovirus at an ultramicroelectrode and its antibody anchoring. Proc Natl Acad Sci. 2015;112:5303–8.
28. Chowdhury AD, De A, Chaudhuri CR, Bandyopadhyay K, Sen P. Label free polyaniline based impedimetric biosensor for detection of E. coli O157: H7 Bacteria. Sens Actuators B Chem. 2012;171:916–23.

29. Chowdhury AD, Gangopadhyay R, De A. Highly sensitive electrochemical biosensor for glucose, DNA and protein using gold-polyaniline nanocomposites as a common matrix. Sens Actuators B Chem. 2014;190:348–56.
30. Chowdhury AD, Takemura K, Li TC, Suzuki T, Park EY. Electrical pulse-induced electrochemical biosensor for hepatitis E virus detection. Nat Commun. 2019;10:3737.
31. Park S, Hwang IW, Makishima Y, Perales-Clemente E, Kato T, Niederländer NJ, Park EY, Terzic A. Spot14/Mig12 heterocomplex sequesters polymerization and restrains catalytic function of human acetyl-CoA carboxylase 2. J Mol Recognit. 2013;26:679–88.
32. Ganganboina AB, Doong R-A. Graphene quantum dots decorated gold-polyaniline nanowire for impedimetric detection of carcinoembryonic antigen. Sci Rep. 2019;9:7214.
33. Raghav R, Srivastava S. Immobilization strategy for enhancing sensitivity of immunosensors: L-Asparagine–AuNPs as a promising alternative of EDC–NHS activated citrate–AuNPs for antibody immobilization. Biosens Bioelectron. 2016;78:396–403.
34. Satoh J, Nishizawa T, Yoshimizu M. Protection against white spot syndrome virus (WSSV) infection in kuruma shrimp orally vaccinated with WSSV rVP26 and rVP28. Dis Aquat Organ. 2008;82:89–96.
35. Torres-Mendieta R, Ventura-Espinosa D, Sabater S, Lancis J, Mínguez-Vega G, Mata JA. In situ decoration of graphene sheets with gold nanoparticles synthetized by pulsed laser ablation in liquids. Sci Rep. 2016;6:30478.
36. Dutta Chowdhury A, Doong R-a. Highly sensitive and selective detection of nanomolar ferric ions using dopamine functionalized graphene quantum dots. ACS Appl Mater Interfaces. 2016;8:21002–10.
37. Dave K, Park KH, Dhayal M. Characteristics of ultrasonication assisted assembly of gold nanoparticles in hydrazine reduced graphene oxide. RSC advances. 2015;5:107348–54.
38. Berzina T, Pucci A, Ruggeri G, Erokhin V, Fontana MP. Gold nanoparticles–polyaniline composite material: Synthesis, structure and electrical properties. Synth Met. 2011;161:1408–13.
39. Cai A, Wang Q, Chang Y, Wang X. Graphitic carbon nitride decorated with S, N co-doped graphene quantum dots for enhanced visible-light-driven photocatalysis. J Alloys Compd. 2017;692:183–9.
40. Mirmohseni A, Solhjo R. Preparation and characterization of aqueous polyaniline battery using a modified polyaniline electrode. Eur Polym J. 2003;39:219–23.
41. Takemura K, Adegoke O, Takahashi N, Kato T, Li T-C, Kitamoto N, Tanaka T, Suzuki T, Park EY. Versatility of a localized surface plasmon resonance-based gold nanoparticle-alloyed quantum dot nanobiosensor for immunofluorescence detection of viruses. Biosens Bioelectron. 2017;89:998–1005.
42. Adegoke O, Morita M, Kato T, Ito M, Suzuki T, Park EY. Localized surface plasmon resonance-mediated fluorescence signals in plasmonic nanoparticle-quantum dot hybrids for ultrasensitive Zika virus RNA detection via hairpin hybridization assays. Biosens Bioelectron. 2017;94:513–22.

Figures

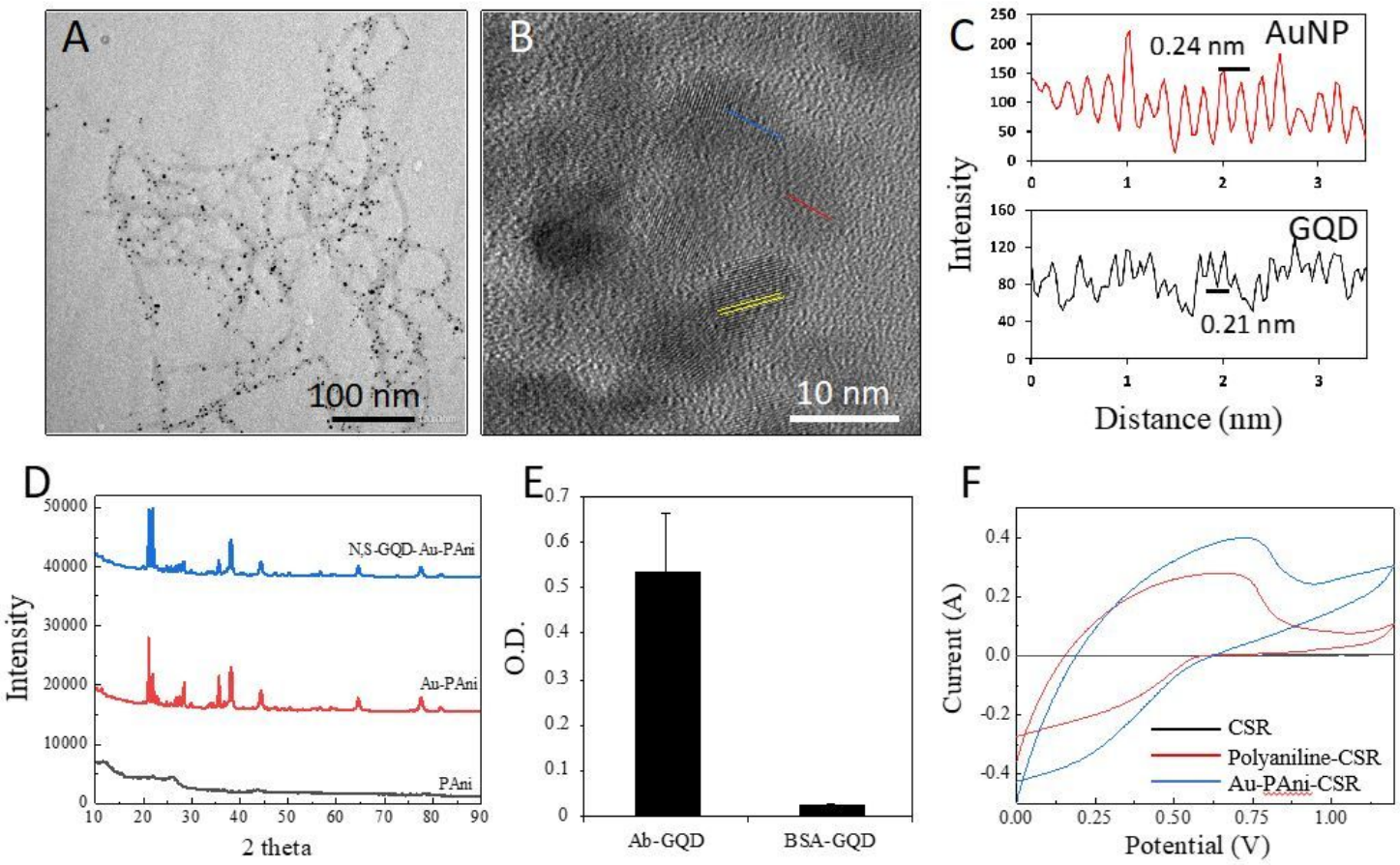

Figure 1

Characterization of Ab-N,S-GQD@AuNP-PAni. (A) TEM image of AuNP-PAni, (B) HR-TEM image of the N,S-GQD-AuNP nanocomposite, and (C) fringe analysis using ImageJ. (D) Powder XRD analysis of silicon, polyaniline silicon, AuNP-PAni@silicon, and N,S-GQD-AuNP-PAni@silicon. (E) ELISA of Ab-N,S-GQDs. (F) Cyclic voltammetry diagrams of CSR, polyaniline-CSR and Au-PAni-CSR.

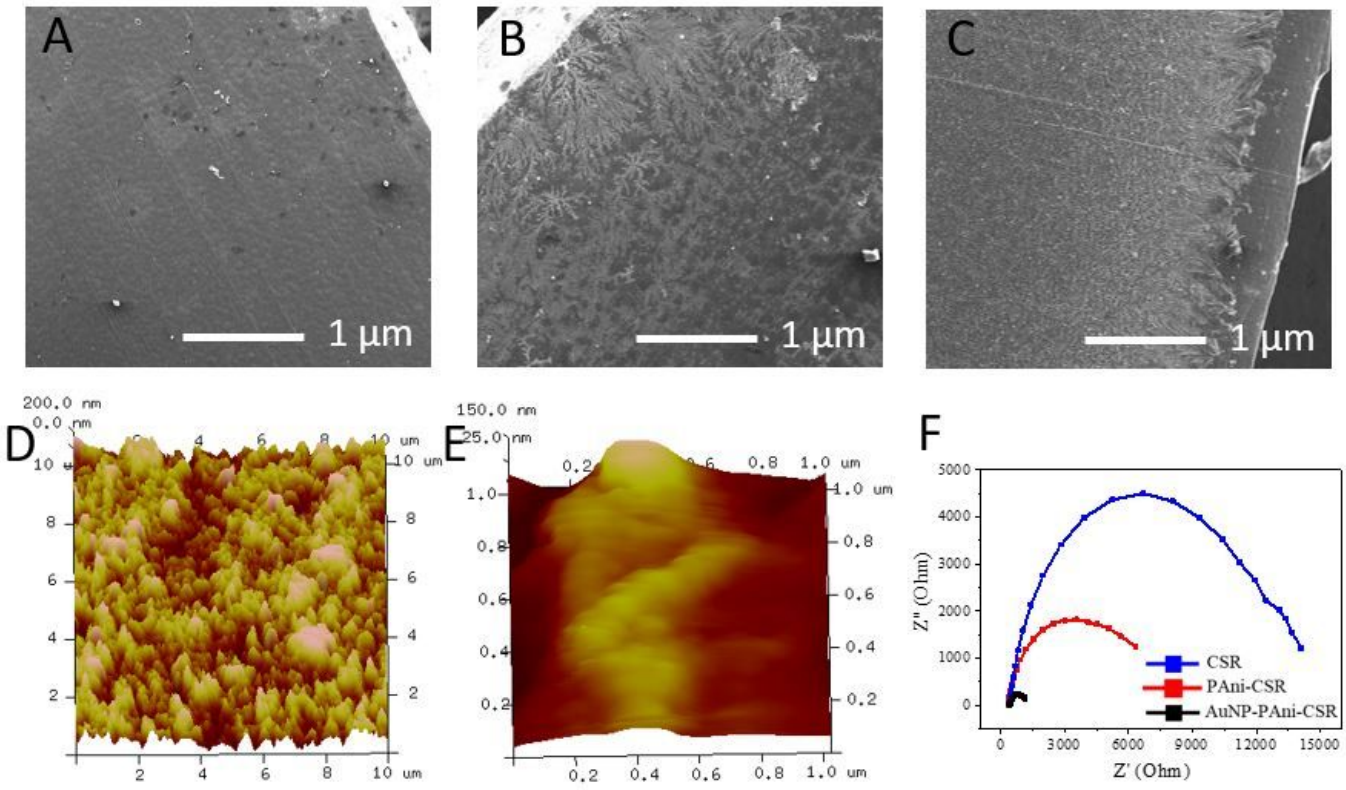

Figure 2

Surface appearances of CSR, PAni-CSR, and AuNP-PAni-CSR. (A—C) SEM images and (D—E) AFM images of CSR and AuNP-PAni-CSR, and (F) impedance Nyquist plot of CSR, PAni-CSR, and AuNP-PAni-CSR.

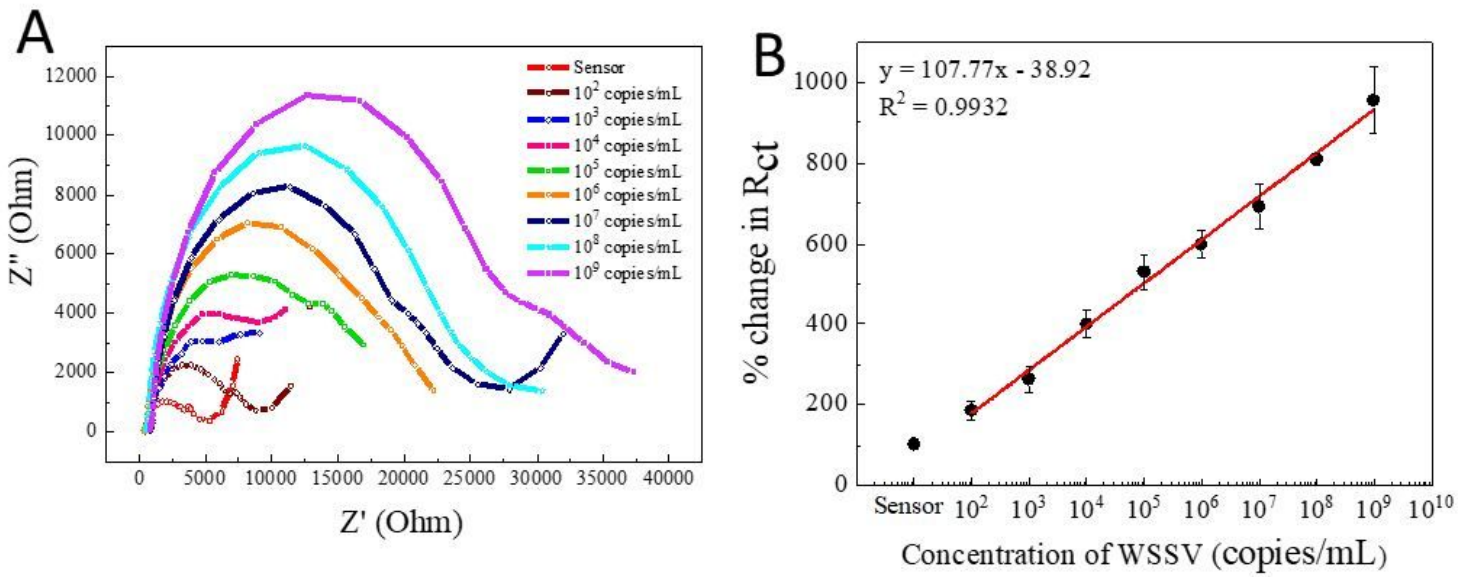

Figure 3

WSSV detection using the disposable electrode. (A) Nyquist plots for different concentrations of WSSV in the range of 102–109 DNA copies/ml. (B) Calibration curve of the corresponding impedance.

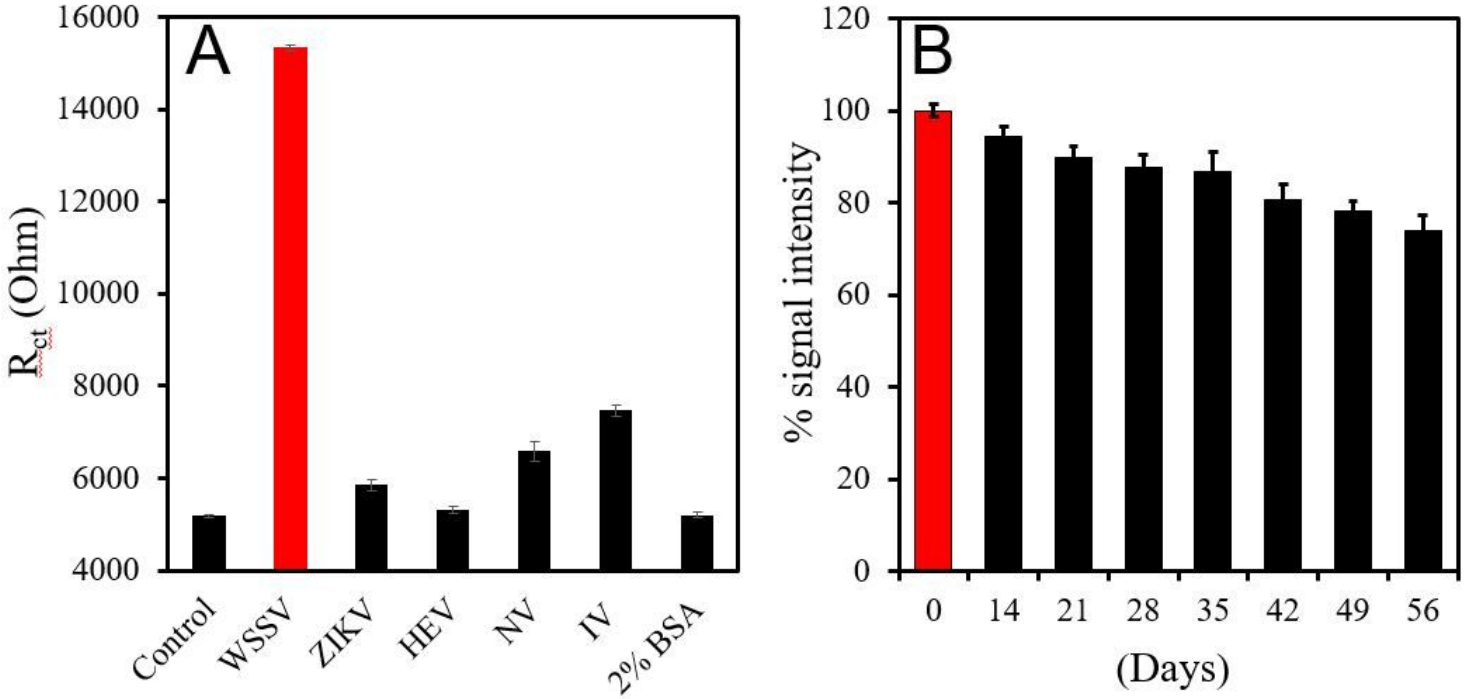

Figure 4

(A) Selectivity test of Ab-N,S-GQD@AuNP-PAni/CSR for WSSV detection compared with nontarget viruses. The concentration of IFV and HEV used was 10 pg/ml, while that of ZIKV and NoV was 104 copies/ml. (B) Stability test of the disposable electrode. The electrode was stored in the refrigerator for 56 d, and the detection performance was investigated every week from the 2nd week. The Rct value on the 0th day was set to 100%.

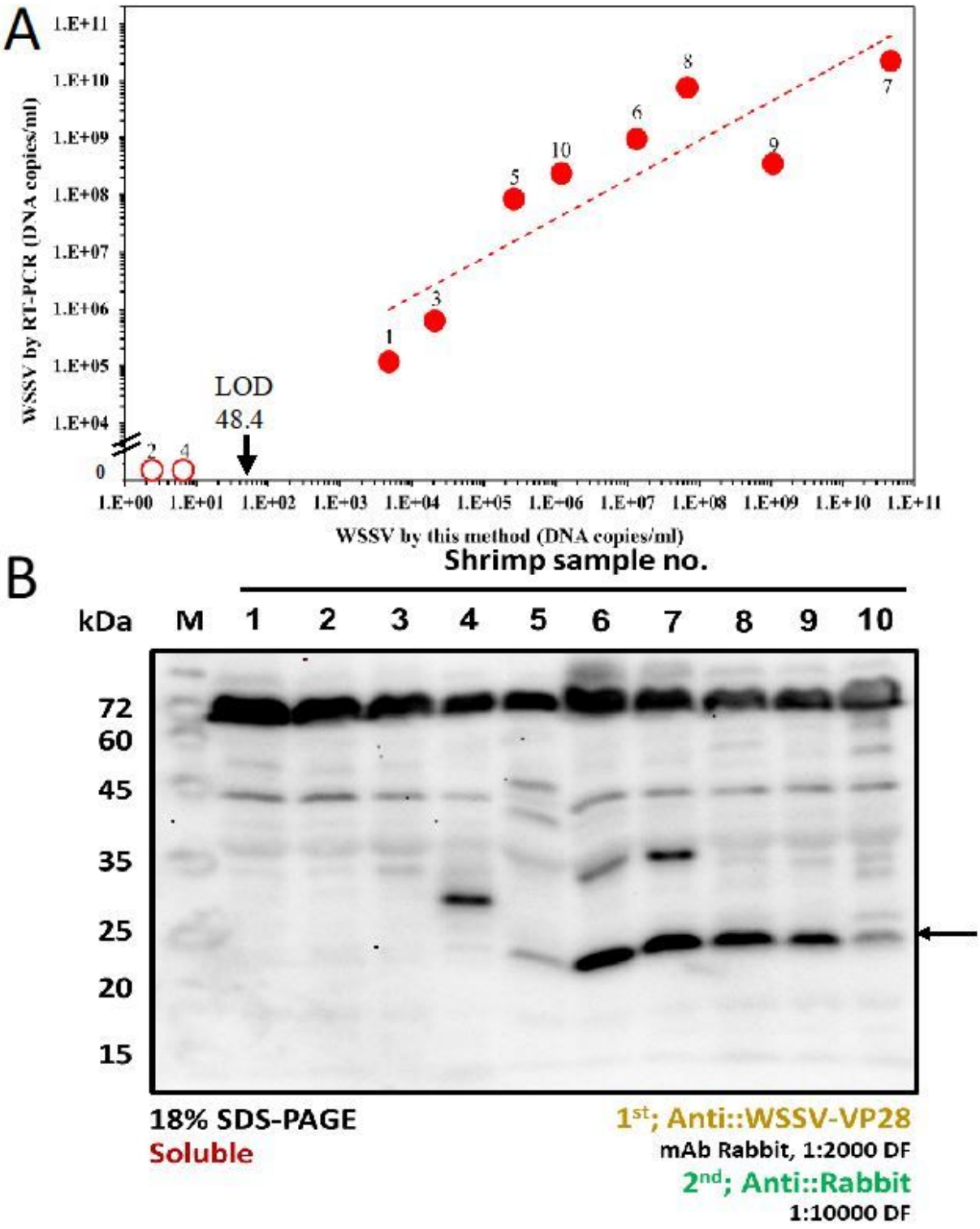

Figure 5

(A) Comparison of electrochemical detection and RT-PCR methods. The open circles (○) indicate a negative and the red circles (●) a positive result as judged by the RT-PCR result. The arrow indicates the limit of detection. (B) Western blot analysis of WSSV-VP28 from shrimp samples using anti-VP28 antibody as a primary antibody. The arrow indicates VP-28.

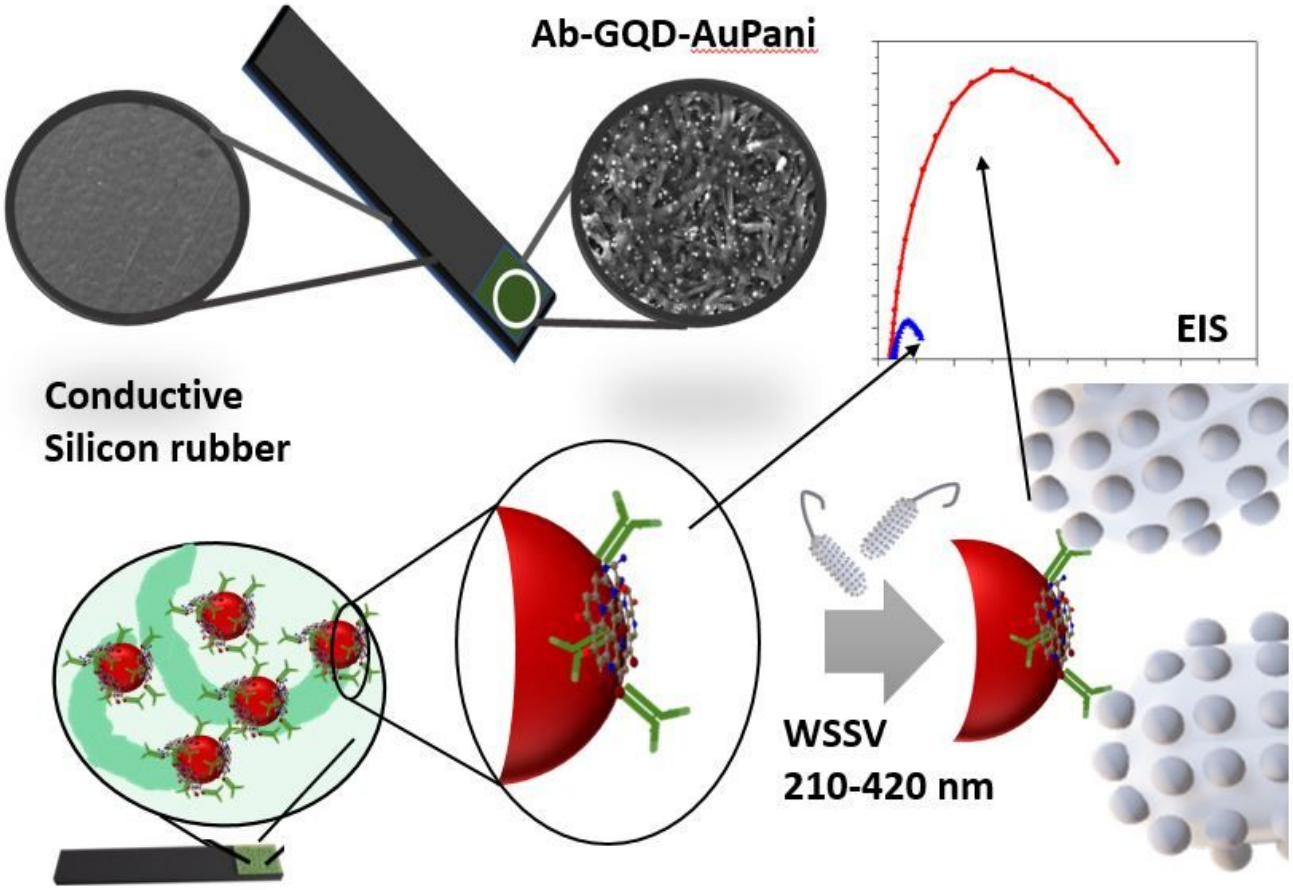

Figure 6

Scheme 1. Overview of a highly conductive disposable electrochemical electrode for the detection of WSSV.

Supplementary Files

This is a list of supplementary files associated with this preprint. Click to download.

- GraphAbstJNAND20291R1.pptx
- SIJNAND20291R1.docx